Hindawi
Mathematical Problems in Engineering
Volume 2021, Article ID 7468963, 14 pages
https://doi.org/10.1155/2021/7468963

Research Article

Real-Time Modeling of Regional Tropospheric Delay Based on Multicore Support Vector Machine

Xu Yang,[1,2,3] **Xinyuan Jiang**,[4] **Chuang Jiang**,[1,2,3] **and Lei Xu**[5]

[1]*School of Spatial Informatics and Geomatics Engineering, Anhui University of Science and Technology, Huainan 232001, China*
[2]*Key Laboratory of Aviation-Aerospace-Ground Cooperative Monitoring and Early Warning of Coal Mining-Induced Disasters of Anhui Higher Education Institutes, Anhui University of Science and Technology, KLAHEI (KLAHEI18015), Huainan 232001, China*
[3]*Coal Industry Engineering Research Center of Mining Area Environmental and Disaster Cooperative Monitoring, Anhui University of Science and Technology, Huainan 232001, China*
[4]*German Research Centre for Geosciences (GFZ), Telegrafenberg, Potsdam 14473, Germany*
[5]*School of Environment Science and Spatial Informatics, China University of Mining and Technology, Xuzhou 221116, China*

Correspondence should be addressed to Xu Yang; xyang@aust.edu.cn and Xinyuan Jiang; xinyuan.jiang@gfz-potsdam.de

Received 7 May 2021; Revised 4 September 2021; Accepted 16 September 2021; Published 4 October 2021

Academic Editor: Amin Jajarmi

Real-time modeling of regional troposphere has attracted considerable research attention in the current GNSS field, and its modeling products play an important role in global navigation satellite system (GNSS) real-time precise positioning and real-time inversion of atmospheric water vapor. Multicore support vector machine (MS) based on genetic optimization algorithm, single-core support vector machine (SVM), four-parameter method (FP), neural network method (BP), and root mean square fusion method (SUM) are used for real-time and final zenith tropospheric delay (ZTD) modeling of Hong Kong CORS network in this study. Real-time ZTD modeling experiment results for five consecutive days showed that the average deviation (bias) and root mean square (RMS) of FP, BP, SVM, and SUM reduced by 48.25%, 54.46%, 41.82%, and 51.82% and 43.16%, 48.46%, 30.09%, and 33.86%, respectively, compared with MS. The final ZTD modeling experiment results showed that the bias and RMS of FP, BP, SVM, and SUM reduced by 3.80%, 49.78%, 25.71%, and 49.35% and 43.16%, 48.46%, 30.09%, and 33.86%, respectively, compared with MS. Accuracy of the five methods generally reaches millimeter level in most of the time periods. MS demonstrates higher precision and stability in the modeling of stations with an elevation at the average level of the survey area and higher elevation than that of other models. MS, SVM, and SUM exhibit higher precision and stability in the modeling of the station with an elevation at the average level of the survey area than FP. Meanwhile, real-time modeling error distribution of the five methods is significantly better than the final modeling. Standard deviation and average real-time modeling improved by 43.19% and 24.04%, respectively.

1. Introduction

Zenith tropospheric delay (ZTD) correction methods can generally be divided into model correction [1], parameter estimation [2], and external correction methods [3]. The parameter estimation method is generally used in precise point positioning (PPP) and long baseline solution, and other methods are needed to obtain ZTD prior value before parameter selection. The external correction method requires expensive equipment and demonstrates difficulty in obtaining accurate results in a short time. The model correction method is the focus of this study.

The ZTD model can be divided into two types, namely, measured meteorological (such as Black, Saastamoinen, and Hopfield models) and empirical (such as GPT series, GZTD, IGGtrop, EGNOS, and UNB models) models, according to whether measured meteorological parameters are needed [4]. Measured meteorological models demonstrate disadvantages of difficult-to-obtain meteorological parameters and low applicability. Empirical models show disadvantages of poor regional

correction effect and dependence on a large number of external grid data. Establishing the ZTD model with nonmeteorological parameters in the region without inputting a large number of external initial data is important in practical application [5, 6]. Time series analysis technologies have been used in previous studies to explore such problems. Dai et al. [7] established a precise troposphere delay model in the Hong Kong region using the calculated troposphere delay of the CORS network for many years. The model takes into account the influence of latitude and elevation of the station and obtains satisfactory results using curve fitting method. ZTD was modeled using the historical ZTD value, and a tropospheric correction prediction model without measured meteorological parameters based on spectrum analysis and autoregressive model (AR) compensation was proposed [8].

In recent years, machine learning (ML) algorithms have been widely used and demonstrated their modeling and predictive accuracy in fields of data mining, pattern recognition, regression, classification, and spatial interpolation. Regional ZTD modeling based on ML method has the advantages of better describing the nonlinear variation law of ZTD, conducting high-precision and high-stability modeling in a large area without actually measuring meteorological parameters and better utilizing meteorological big data for data mining. It is successfully employed in ZTD modeling to overcome the shortcomings of the above two types of ZTD models; A GPS tropospheric delay interpolation model based on radial basis function (RBF) neural network was constructed, and the accuracy of tropospheric delay interpolation of the model can reach the millimeter level with CORS station data of Anhui power system [9]. A fusion model was proposed to compensate for errors in prediction of ZTD, by incorporating back-propagation neural network (BPNN). Modeling results from the Hopfield and proposed model were compared by reference to the true ZTD. It showed that the proposed model could improve ZTD prediction accuracy by more than 90% [10]. The traditional BPNN model was initialized with rich regional long-term continuously operating reference stations (CORS) information to reduce model parameters. The experimental results with National Center for Atmospheric Research (NCAR) troposphere data showed that the improved BPNN model demonstrates remarkable improvement in fitting and prediction accuracy [11]. A regional fusion model with BPNN and genetic algorithm that obtains high accuracy (57% higher than EGNOS) and independent of large external amounts of initial data was established on the basis of the EGNOS model [12]. A method of tropospheric delay interpolation estimation for long baseline network real-time kinematic (RTK) based on support vector machine (SVM) theory was proposed. The experimental results showed that the tropospheric delay accuracy of the interpolation estimation was better than 2 cm, and the estimation error was generally stable [13]. Compared with the traditional BPNN algorithm, the advantage and feasibility of the proposed regional ZTD model based on least squares support vector machine algorithm using global navigation satellite system (GNSS) and ERA5 Data were investigated in [14]. Regional ZTD modeling based on ML method has important applications in real-time precise positioning, real-time ZTD vertical profile inversion, atmospheric water vapor parameter inversion, extreme weather forecast, regional InSAR deformation monitoring, and so on. A method based on a relevance vector machine was developed for retrieving atmospheric refractivity profiles in real time from the slant path tropospheric delay at low elevations (<5°) of a single ground-based GPS receiver. The simulation and experiment results showed that the retrieving profiles based on the proposed method were better than those obtained by Lowry's method and the Hopfield model [15]. Sangiorgio et al. [16] implemented advanced deep learning predictors, such as the deep neural nets (DNNs), for the forecasting of the occurrence of extreme rainfalls. The experimental result showed that the DNN with ZTD model accuracy improved 10%, compared with the traditional logistic regression without ZTD model. Shamshiri et al. [17] proposed a new technique based on ML Gaussian processes (GP) regression approach using the combination of small-baseline interferograms and GNSS derived ZTD values to mitigate phase delay caused by troposphere in interferometric observations, exploiting roughly 200 permanent GNSS stations (CPOS) provided by the Norwegian mapping authority (NMA).

Regional ZTD modeling products can improve precise point positioning (PPP) performance, which is of great significance to PPP application research. Yao et al. [18] established a global nonmeteorological parameter ZTD model with an external coincidence accuracy of about 4 cm. By using the ZTD obtained from the model as the virtual observation of PPP model, the PPP convergence time can be improved up to 15% [19]. Li's research [20] showed that when the regional ZTD interpolation (40 km scale) accuracy was less than 1 cm, it could meet the demand of PPP for instantaneous ambiguity resolution. Dai's research [21] showed that for the regional tropospheric modeling with the four-parameter method, the accuracy of small region modeling (40 km scale) was 1 cm, and the accuracy of large region (300 km scale) was 2 cm. Single-frequency and dual-frequency PPP performance could be significantly improved by using the atmospheric correction products.

The real-time ZTD of each CORS station is calculated with real-time PPP technology based on the variance component in [22] to realize the practical application of the model without measured meteorological parameters, and Hong Kong regional CORS (15 km scale) is used as an example. The real-time modeling of ZTD in the Hong Kong region is carried out with multicore support vector machine (MS) based on genetic optimization algorithm, single-core support vector machine (SVM), four-parameter method (FP), neural network method (BP), and root mean square fusion method (SUM). The model accuracy is evaluated, and the real-time and high-precision regional ZTD model is further studied using artificial intelligence technology.

2. Regional Real-Time Tropospheric Delay Modeling Principle

2.1. Support Vector Machine Modeling

2.1.1. Basic Principles of Support Vector Machines. Cortes and Vapnik first proposed SVM on the basis of Vapnik–Chervonenkis theory in structural risk minimization and

statistics and originally used to solve the problem of computer pattern recognition [23]. SVM is a "small sample" learning method that can avoid limitations of other machine learning methods, such as underlearning, high dimensionality, and easy to fall into local optimality, and can be used in a regression analysis called support vector regression (SVR).

SVR primarily defines a loss function, establishes a corresponding kernel function, maps the original data space to a high-dimensional space through nonlinear transformation, converts the regression function problem into a quadratic convex optimization problem, introduces relaxation factors and penalty coefficients to form a dual optimization problem, and finally obtains the optimal solution of the optimization problem [24]. The SVR principle is expressed as follows.

The training sample set is assumed $\{(x_i, y_i), i = 1, 2, \ldots, l\}$. The number of samples is equal to l. $x_i \in \mathrm{R}^N$ and $y_i \in \mathrm{R}$ are input and target values, respectively. Insensitive loss function ε can be expressed as follows:

$$L(y, f(x)) = |y - f(x)|_\varepsilon = \begin{cases} 0, & |y - f(x)| \le \varepsilon, \\ |y - f(x)| - \varepsilon, & |y - f(x)| > \varepsilon. \end{cases} \tag{1}$$

The regression estimation function $f(x)$ in formula (1) can be constructed in the following form after learning from sample sets:

$$f(x) = w \bullet \psi(x) + b, \tag{2}$$

where $\psi(x)$ is the nonlinear function that maps x to a linear feature space of dimension w (possibly infinite dimension).

The objective problem of the sample (x_i, y_i) and the estimated function becomes the following convex quadratic programming problem:

$$\min_{w,b,\xi} \frac{1}{2}\|w\|^2 + \gamma \sum_{i=1}^{l} (\xi_i + \xi_i^*)$$
$$\text{s.t.} \begin{cases} y_i - w \cdot \psi(x_i) - b \le \varepsilon + \xi_i, \\ w \cdot \psi(x_i) + b - y_i \le \varepsilon + \xi_i^*, \end{cases} \tag{3}$$

where $\xi_i \ge 0, \xi_i^* \ge 0$ are slack variables and γ is the penalty factor. The following regression estimation function is obtained by solving formula (3) with the Lagrangian multiplier method:

$$f(x) = \sum_{x_i \in \mathrm{SV}} (\alpha_i - \alpha_i^*) K(x_i, x) + b, b = \frac{1}{N_{\mathrm{NSV}}} \left\{ \sum_{0 < \alpha_i < \mathrm{C}} \left[y - \sum_{x_j \in \mathrm{SV}} (\alpha_j - \alpha_j^*) K(x_j, x_i) - \varepsilon \right] + \sum_{0 < \alpha_i^* < \mathrm{C}} \left[y_i - \sum_{x_j \in \mathrm{SV}} (\alpha_j - \alpha_j^*) K(x_j, x_i) + \varepsilon \right] \right\}, \tag{4}$$

where α_i, α_i^* are Lagrange multipliers. x_i corresponding to nonzero α_i or α_i^* obtained by the optimization calculation is called the support vector, and only the support vector contributes to w, that is, contributes to the estimation function $f(x)$. SV and N_{NSV} are the support vector set and the standard support vector number, respectively, and $K(x_i, x_j)$ is the kernel function.

2.1.2. Selection of Multicore Functions and Their Parameters. The performance of SVM depends on the selection of the kernel function and its parameters. However, many types of kernel functions exist, each with its own characteristics, advantages, and disadvantages. Therefore, if a single kernel function is used to solve the actual problem, then the classification performance of SVM is often nonoptimal with certain limitations. Moreover, constructing corresponding kernel functions on the basis of actual problems is often necessary in addition to using common single kernel functions (such as polynomial, Gaussian, Sigmoid, and linear kernel functions). Therefore, combining different kernel functions for learning can be considered to select a suitable kernel function. The multicore function $K_{\mathrm{mk}}(x_i, x_j)$ can be expressed as follows [25]:

$$K_{\mathrm{mk}}(x_i, x_j) = \sum_{r=1}^{m} p_r \cdot K_{\mathrm{local}}^r(x_i, x_j) + \sum_{t=1}^{n} p_t \cdot K_{\mathrm{global}}^t(x_i, x_j), \tag{5}$$

where $K_{\mathrm{local}}^r(x_i, x_j)$ and $K_{\mathrm{global}}^t(x_i, x_j)$ represent r-th local and t-th global kernel functions, respectively, m and n are the number of local and global kernel functions, respectively, and the fusion coefficient of each kernel function satisfies $0 \le p_1, p_2, \ldots, p_r, \ldots, p_m \le 1$, $0 \le p_1, p_2, \ldots, p_t, \ldots, p_n \le 1$, $\sum_{r=1}^{m} p_r + \sum_{t=1}^{n} p_t = 1$.

The local kernel function demonstrates strong learning but weak generalization abilities. The global kernel function exhibits strong generalization but weak learning abilities. The hybrid kernel function shows both local and global characteristics and certain learning and generalization abilities. Commonly used local and global kernel functions selected in this study are radial basis and polynomial kernel functions, respectively, which are expressed as follows:

$$K(x_i, x_j) = \exp\left(\frac{-|x_i - x_j|^2}{\sigma^2} \right), \tag{6}$$

$$K(x_i, x_j) = (a x_i^T x_j + c)^q, \tag{7}$$

where σ, a, c, and q are kernel parameters that satisfy σ, $a > 0$, $c \geq 0$, and $q \in \mathrm{N}$, respectively.

Formulas (5)–(7) showed that extrapolation ability of the radial basis kernel function decreases with the increase of the parameter σ when selecting kernel parameters. A large parameter q indicates high mapping dimension and computational workload. Learning complexity will be excessively high and the phenomenon of "overfitting" will likely occur when q is overly large. The multikernel function clearly degenerates into a single kernel function when the fusion coefficient of a certain kernel function is 1 and that of other kernel functions is 0. The model parameter selection of the SVR machine based on a single kernel function is the only selection of internal parameters of the single kernel function. The model parameter selection of the SVR machine with multicore function as the core should select not only internal parameters of the local kernel function but also those of the global kernel function while determining fusion coefficients of all kernel functions to ensure that the performance of the SVR machine based on the multikernel function is optimal [26, 27].

Manually selecting these parameters is evidently time consuming and laborious, and optimal results cannot be guaranteed. Hence, choosing an acceptable optimization algorithm is very important. Commonly used parameter optimization algorithms include grid search, genetic algorithm, and particle swarm algorithm. Genetic optimization algorithm [28], which uses a probabilistic optimization method, is selected in this study. This algorithm can automatically obtain and guide the optimized search space, adjust the search direction adaptively without needing definite rules, and demonstrate characteristics of inherent implicit parallelism and enhanced global optimization ability. Calculation steps of the genetic algorithm mainly include initialization, selection, crossover, mutation, and global optimal convergence.

2.2. Other Modeling Methods. Other widely used modeling methods, such as FP [29], BP neural network [11], SVM with radial basis kernel function [24], and SUM, which is a simple fusion of the first three methods, are also used to compare and analyze the effect of multicore SVM modeling.

Searching for three stations closest to the user location; obtaining the ZTD results of the three stations with the three model algorithms of FP, BP, and SVM; and analyzing the root mean square error (RMS) of each of the three model algorithms can summarize the basic principle of SUM modeling. Weights under the results of the three model algorithms being fused are obtained according to the RMS weighting method. The respective weights of the three model algorithms decrease with the increase of the RMS when their results are fused. Specific modeling steps are presented as follows:

(1) Search the nearest three stations as verification points according to the user's input coordinate position.

(2) Sequentially delete verification point data from the original data and use the above three models to calculate the ZTD of the verification point on the basis of remaining data.

(3) Compare the calculation result with the original data and calculate the deviation and RMS, which is expressed as follows:

$$\mathrm{RMS}_i = \sqrt{\frac{\left(\mathrm{bias}_1^2 + \mathrm{bias}_2^2 + \mathrm{bias}_3^2\right)}{3}}, \tag{8}$$

where RMS_i represents the RMS error (RMSE) of the i-th modeling method and *bias* represents the deviation between the calculated value of the ZTD and the actual value.

(4) Calculate the weight with the RMSE of each method as follows:

$$w_i = \frac{\mathrm{RMS}_i^{-p}}{\sum_{i=1}^{3} \mathrm{RMS}_i^{-p}}, \quad (i = 1, 2, 3;\ p = 2), \tag{9}$$

where ω_i is the weight of the first algorithm and p is the power value (usually 1 or 2, and this article uses 2). A large power value indicates a large weight of the result with a small RMS_i.

(5) Obtain the ZTD value of the user input coordinate position with the three algorithms and then calculate the weighted average as the optimal ZTD, which is expressed as follows:

$$\mathrm{ZTD} = \sum_{i=1}^{3} w_i \times \mathrm{ZTD}_i, \quad (i = 1, 2, 3), \tag{10}$$

where ZTD_i is the ZTD calculated via the i-th modeling method.

2.3. Elevation Naturalization. Tropospheric wet delay is strongly related to altitude. The elevation of the station must be considered in tropospheric modeling to avoid a deviation of several centimeters [30]. The exponential function used in [18] is selected in this study for establishing the GZTD global tropospheric model to describe the law of ZTD change with elevation as follows:

$$\mathrm{ZTD}(h) = \mathrm{ZTD}_i \times \exp\left(-\frac{1}{H} \times (h - h_i)\right), \tag{11}$$

where h is the altitude of the point to be determined, ZTD_i represents the ZTD value of the known point, and h_i is the corresponding altitude. Altitude H is the only unknown parameter in the process of transmitting tropospheric correction information from the known point to the point to be determined. Let $A = 1/H$ for ZTD data of the station, and the least square algorithm can be used to solve A. ZTD of the point to be determined is then calculated.

The process of real-time or final ZTD modeling in this article is shown in Figure 1.

In this paper, the ZTD modeling is completed under the software MATLAB 2017a. The MATLAB toolboxes of MS, SVM, and BP, and SUM models are LIBSVM, SVM, and

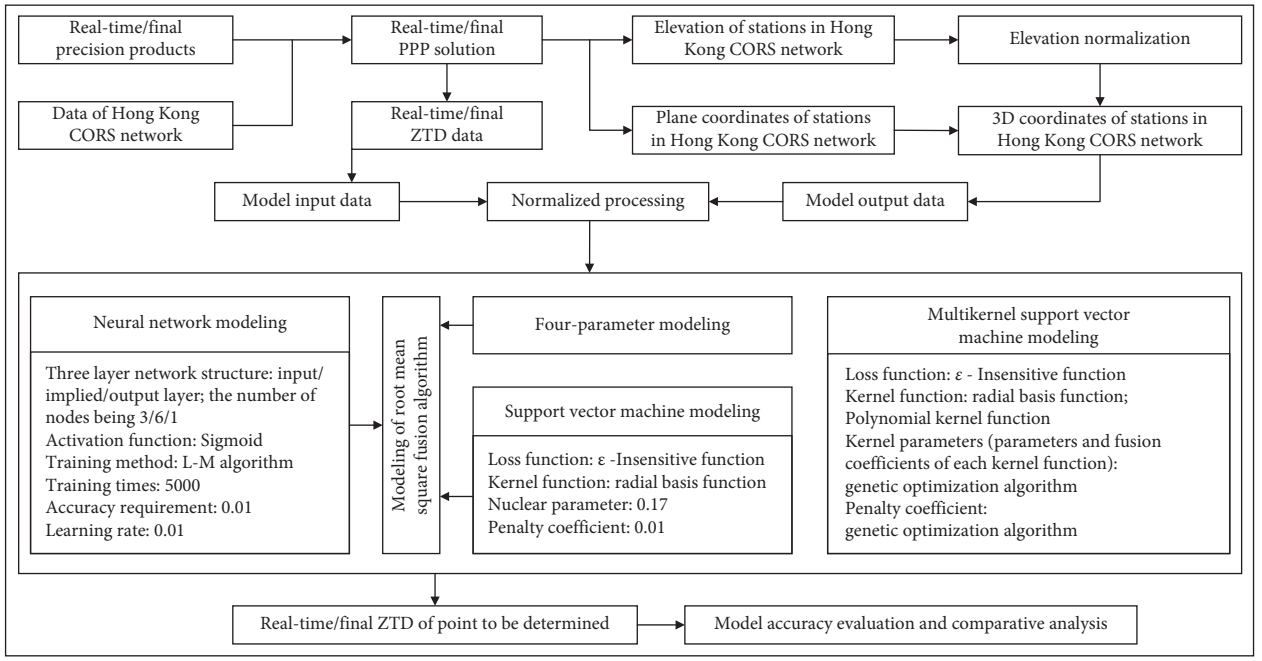

Figure 1: Real-time or final ZTD modeling process.

neural network, respectively. The ZTD models can be delivered to real-time PPP users after taking the ZTD modeling process and modeling products as a submodule of a real-time PPP service system [31] and establishing data communication between the service system and the submodule. The realization process is as follows. Firstly, the data needed for modeling is obtained in real time from the service system through Internet. Then, the ZTD modeling is carried out, and the real-time ZTD modeling products are transmitted to the service system through Internet. Finally, the service system broadcasts real-time precision products, including satellite orbit, clock offset, and atmospheric error corrections, to real-time PPP users through Internet or navigation messages.

3. Comparative Analysis of FP/BP/SVM/SUM/MS Modeling of Regional Real-Time or Final Tropospheric Delay

3.1. Data Source. Five days (January 16–20, 2019) of four-system observation data from 19 reference stations in the Hong Kong CORS network are used with a data sampling interval of 30 s. Figures 2 and 3 show station and their elevation distributions, respectively. Final and real-time ZTD data with a sampling interval of 30 s for each reference station are obtained from the PPP solution in the GRCE mode based on variance component estimation in Reference [22]. The product of orbit with a sampling interval of 5 min and satellite clock offset with a sampling interval of 30 s used in the final PPP solution is the final multi-GNSS precise product "GBM" from German Research Centre for Geosciences (GFZ). The product of the orbit with a sampling interval of 5 s and the satellite clock offset with a sampling interval of 5 s used in the real-time PPP solution is the real-time multi-GNSS precise product "CLK93" from

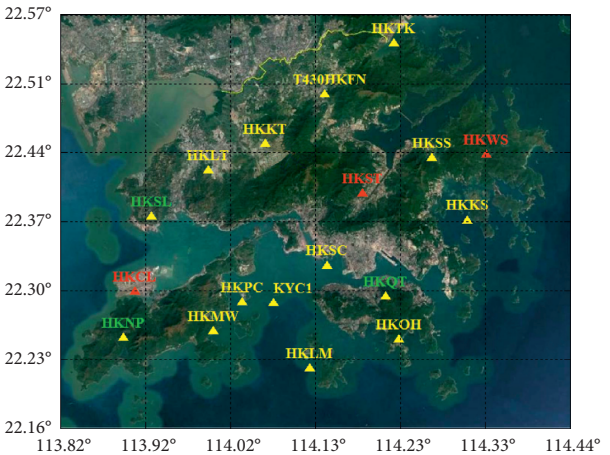

Figure 2: CORS network station distribution map.

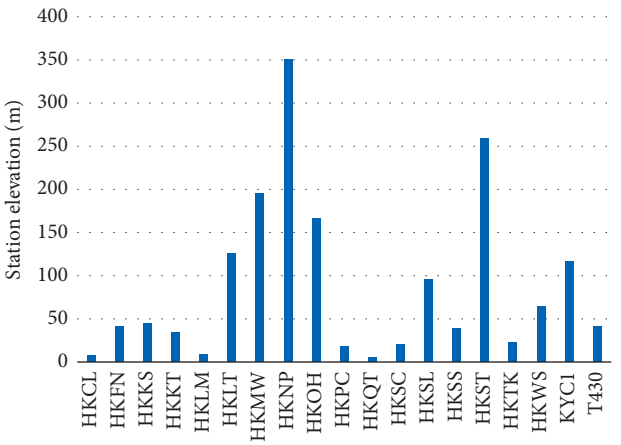

Figure 3: CORS network station elevation distribution map.

Centre National d'Etudes Spatiales (CNES). Missing parts of real-time orbit products are filled with GFZ ultrafast predicted orbits with Lagrangian interpolation. The missing part of the real-time clock offset is supplemented using the real-time clock offset prediction method in [32]. The PPP solution software is independently developed. The software-specific parameter configuration and processing strategy are shown in Table 1. Figure 2 shows that 16 stations marked by yellow triangles are used for modeling, 3 stations marked by red triangles are used for accuracy verification, and 3 stations marked in green text denote internal accuracy check stations for modeling among the 16 base stations. Real-time and final ZTD values of 19 stations for five consecutive days are calculated according to the sampling interval of 30 s before modeling. ZTD fitting and forecasting of regional stations are performed according to the sampling interval of 5 min during the modeling process. The modeling results of the first two hours of each day are removed when performing model fitting and forecast accuracy statistics to reduce the influence of PPP convergence on the ZTD solution results. That is, 264 epoch fitting or forecast data participate in the statistical analysis of model accuracy in a day for a certain station among the 19 stations.

Three indicators, namely, standard deviation (STD), RMSE, and average deviation (bias), are used to evaluate the modeling effect. The experimental results of [22] showed that the real-time ZTD solution (10 mm) and final ZTD (6 mm) accuracy levels reach the average level obtained by many studies. Therefore, the calculated ZTD value can be used as the true value to evaluate the accuracy level of real-time and final ZTD modeling in this study. Accuracy indicators of bias, RMSE, and STD are calculated as follows [11]:

$$\text{Bias}^{\text{true}} = \frac{1}{N_2}\sum_{i=1}^{N}\left(\text{ZTD}_i^{\text{model}} - \text{ZTD}_i^{\text{true}}\right), \tag{12}$$

$$\text{Bias}^{\text{observ}} = \frac{1}{N_1}\sum_{i=1}^{N}\left(\text{ZTD}_i^{\text{model}} - \text{ZTD}_i^{\text{observ}}\right), \tag{13}$$

$$\text{RMSE} = \sqrt{\frac{\sum_{i=1}^{N}\left(\text{ZTD}_i^{\text{model}} - \text{ZTD}_i^{\text{true}} - \text{Bias}^{\text{true}}\right)^2}{N_2}}, \tag{14}$$

$$\text{STD} = \sqrt{\frac{\sum_{i=1}^{N}\left(\text{ZTD}_i^{\text{model}} - \text{ZTD}_i^{\text{observ}} - \text{Bias}^{\text{observ}}\right)^2}{N_1}}, \tag{15}$$

where N_1 and N_2 are the number of fitting and forecast samples, respectively, and $\text{ZTD}_i^{\text{model}}$, $\text{ZTD}_i^{\text{observ}}$, and $\text{ZTD}_i^{\text{true}}$ are the model solution, observation, and known values of the i-th measurement, respectively. *Bias* can appropriately reflect the presence of system errors in the model. RMSE can reflect the distribution of the difference between observed and true values. STD measures the degree of dispersion of the measurement error distribution.

3.2. Result Analysis. Three stations (HKQT (5.15 m), HKSL (95.28 m), and HKNP (350.67 m)) participating in modeling are selected to analyze the fitting accuracy of the model. Stations unrelated to the modeling (HKCL (7.73 m), HKWS (63.77 m), and HKST (258.70 m)) are used to analyze the forecast accuracy of the model. There are obvious differences in the elevation of the first or last three stations.

3.2.1. Final ZTD Modeling Analysis. ZTD of each station calculated using the final PPP solution is taken as the true value, and the accuracy of various models is evaluated. Figure 4 shows the daily fitting and forecast accuracy statistics results of the FP, BP, SVM, SUM, and MS models. Accuracy statistics of five consecutive days for the five models are listed in Table 2.

The following can be deduced from Figure 4 and Table 2:

(a) The fitting and prediction accuracy of the five models all demonstrate a certain relationship with the elevation of the station. The HKCL station with lower elevation shows the lowest prediction accuracy and the HKQT station with lowest elevation exhibits lower fitting accuracy but still higher than HKCL mainly because the tropospheric wet delay of the station with lower elevation changes significantly and the water vapor around the HKCL station changes significantly given that the area is near the sea. The fitting or prediction accuracy of the four other stations demonstrates no significant difference. The decrease in modeling accuracy of the station with high elevation is insignificant.

(b) The daily modeling accuracy of the BP model demonstrates a slightly greater change than the four other modeling methods primarily due to

Table 1: Real-time PPP estimation strategy.

Parameter		Handling strategy
Observation information	Observation	LC, PC
	Elevation mask angle	5°; height angle weight determination
	Phase wing-up	Model correction
	Phase center change	IGS08 model
Error correction	Tide correction	Model correction (solid and ocean tide)
	Satellite phase center	Absolute phase center
	Relativistic correction	Model correction
	Satellite clock offset	GBM precise clock and CLK93 real-time clock
	Satellite orbit	GBM precise orbit and CLK93 real-time orbit
	ERPs	GBM IERS products
Parameter estimation	Site coordinates	Estimated as constant for each epoch
	Troposphere	Estimated, UNB3m model + random walk/VCE
	System time offset	Estimated as white noise for each epoch
	Receiver clock biases	Estimated as white noise for each epoch
	Ambiguity	Estimated as constant for each ambiguity arc

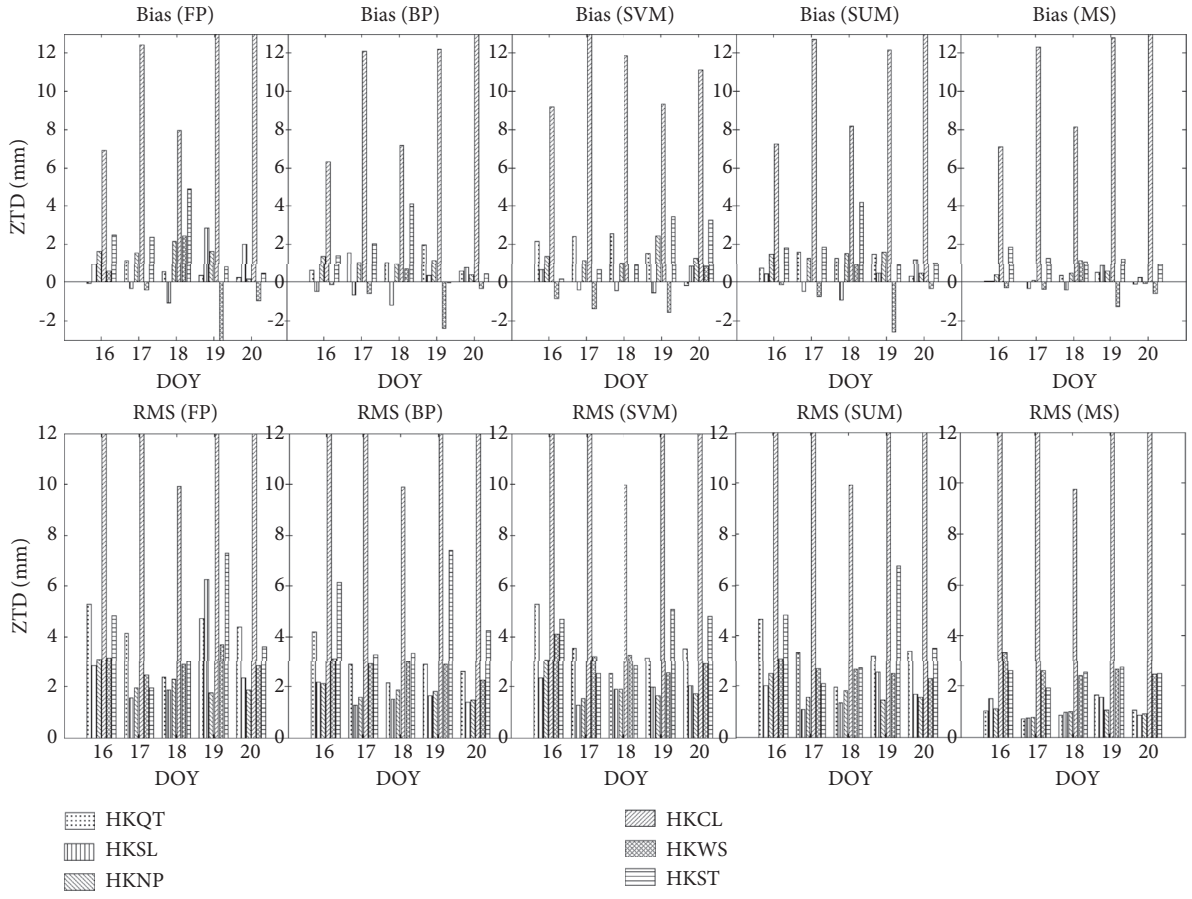

Figure 4: ZTD daily fitting and prediction accuracy statistics results of the five models. Note that bias in the figure refers to $\text{Bias}^{\text{ture}}$ in formula (12) or $\text{Bias}^{\text{observ}}$ in formula (13). RMS refers to RMSE in formula (14) or STD in formula (15), and the meaning in the following figures is similar.

insufficient training samples that causes the unstable characteristic of the model. The accuracy of FP modeling within a day is lower than that of the four other modeling methods. The ZTD modeling experiment results of six observation stations for five consecutive days showed that the average bias and RMS values of FP, BP, SVM, and SUM reduced by 53.80%, 49.78%, 25.71%, and 49.35% and 40.70%,

Table 2: ZTD fitting and forecast accuracy statistics results of five consecutive days for the five models.

Modeling method	$Bias^{observ}$ (mm)			$Bias^{true}$ (mm)			STD (mm)			RMSE (mm)		
	HKQT	HKSL	HKNP	HKCL	HKWS	HKST	HKQT	HKSL	HKNP	HKCL	HKWS	HKST
FP	0.43	0.88	1.43	10.93	−0.47	2.21	4.17	2.96	2.18	15.51	2.99	4.12
BP	1.14	−0.26	0.98	10.31	−0.56	1.60	2.93	1.59	1.76	15.46	2.82	4.88
SVM	1.69	0.00	1.45	11.09	−0.60	1.67	3.60	1.90	1.96	15.63	3.19	3.98
SUM	1.06	0.12	1.27	10.77	−0.59	1.95	3.30	1.72	1.76	15.41	2.62	3.97
MS	0.14	0.06	0.28	10.79	−0.29	1.27	1.05	1.12	0.97	15.47	2.68	2.44
Mean	0.89	0.16	1.08	10.78	−0.50	1.74	3.01	1.86	1.73	15.49	2.86	3.88

32.30%, 36.40%, and 30.67%, respectively, compared with those of MS.

(c) All five modeling methods demonstrate high accuracy. The minimum, maximum, and average values of average bias for five consecutive days, except for the HKCL station, are 0.0022 (SVM), 2.21 (FP), and 0.67 mm, respectively. The minimum, maximum, and average values of average RMS are 0.97 (MS), 4.88 (BP), and 2.67 mm, respectively.

3.2.2. Real-Time ZTD Modeling Analysis. After real-time ZTD modeling of the six stations, ZTD of each station calculated using the final PPP solution is taken as the truth value to evaluate the accuracy of various models. Accuracy statistics of the five models for five consecutive days are listed in Table 3.

The following can be deduced from Table 3:

(a) Relatively poor modeling effects of HKCL and HKQT stations and nearly the same modeling effects of the four remaining stations indicate the similar modeling effects of the five modeling methods in real-time and final ZTD modeling.

(b) Compared with the results in Table 1, the absolute deviation, average deviation, and RMS of real-time ZTD modeling are generally larger than those of the final ZTD modeling. This finding indicated that a certain level of difference in accuracy exists between real-time and final ZTD modeling results. This phenomenon is consistent with the results of previous studies.

(c) Compared with the four other models, MS demonstrates certain improvements in the fitting and prediction accuracy. The difference in modeling effects of the four other models is insignificant. The RMS of SVM model is slightly better than the three other models. Average deviations and RMS of the five models of the stations, except for the HKCL station, are 1.32 and 9.10 mm, respectively.

3.2.3. Comparative Analysis of Real-Time and Final ZTD Modeling. ZTD of each station calculated using real-time PPP technology is taken as the true value, and the accuracy of various models is reevaluated to analyze characteristics of real-time ZTD modeling further. The daily fitting and forecast accuracy statistical results of FP, BP, SVM, SUM, and MS models are illustrated in Figure 5. Accuracy statistics of the five models for five consecutive days are presented in Table 4. Real-time and final ZTD modeling error distributions are compared and analyzed. Real-time and final ZTD error changes of six stations for five consecutive days are shown in Figure 6, and their error distributions are illustrated in Figure 7.

The following can be deduced from Figure 5 and Table 4:

(a) The fitting and prediction accuracy of the five models all demonstrate a certain relationship with the elevation of the station.

(b) The daily modeling accuracy of the BP model exhibits a slightly greater change than the four other modeling methods. The ZTD modeling experiment results of six observation stations for five consecutive days showed that the average bias and RMS values of FP, BP, SVM, and SUM reduced by 48.25%, 54.46%, 41.82%, and 51.82% and 43.16%, 48.46%, 30.09%, and 33.86%, respectively, compared with those of MS.

(c) All five modeling methods show high accuracy. Minimum, maximum, and average values of average Bias for five consecutive days, except for the HKCL station, are 0.04 (SVM), 3.15 (SVM), and 1.09 mm, respectively. Minimum, maximum, and average values of average RMS are 0.22 (MS), 2.03 (BP), and 1.18 mm, respectively.

The following can be deduced from Figures 6 and 7 and Tables 2 and 4:

(a) Tables 2 and 4 and Figure 6 showed that the bias and fitting accuracy of the MS model significantly improve compared with those of the four other models. The MS model demonstrates clear advantages over the four other models, especially for the modeling of stations with elevation at the average level and higher elevation of the survey area. RMS of FP, BP, SVM, and SUM for the final modeling of HKSL and HKNP stations reduces by 58.99%, 37.43%, 45.90%, and 39.93%, respectively, compared with that of MS. RMS of FP, BP, SVM, and SUM for the real-time modeling of HKSL and HKNP stations reduces by 67.35%, 71.09%, 60.99%, and 60.73%, respectively, compared with that of MS. RMS of FP, BP, SVM, and SUM for the final modeling of HKWS and HKST stations reduces by 28.03%, 22.55%, 25.91%, and

Table 3: Final ZTD fitting and forecast accuracy statistical results of the five models for five consecutive days, with the final ZTD as the true value.

Modeling method	$\text{Bias}^{\text{true}}$ (mm)						RMSE (mm)					
	HKQT	HKSL	HKNP	HKCL	HKWS	HKST	HKQT	HKSL	HKNP	HKCL	HKWS	HKST
FP	0.27	1.49	2.83	11.06	−0.19	3.42	11.85	8.04	9.25	19.04	8.81	7.85
BP	−0.02	1.30	1.91	10.49	−0.69	3.27	11.70	8.31	9.57	19.21	8.72	7.84
SVM	0.72	1.70	2.76	12.05	−0.70	2.49	11.69	8.19	9.22	19.32	8.66	7.65
SUM	0.31	1.56	2.47	11.06	−0.61	3.05	11.75	8.18	9.35	19.16	8.75	7.76
MS	0.15	1.21	1.23	11.06	−0.02	3.05	10.95	8.02	9.18	19.02	8.68	7.58
Mean	0.29	1.45	2.24	11.14	−0.44	3.06	11.59	8.15	9.31	19.15	8.72	7.74

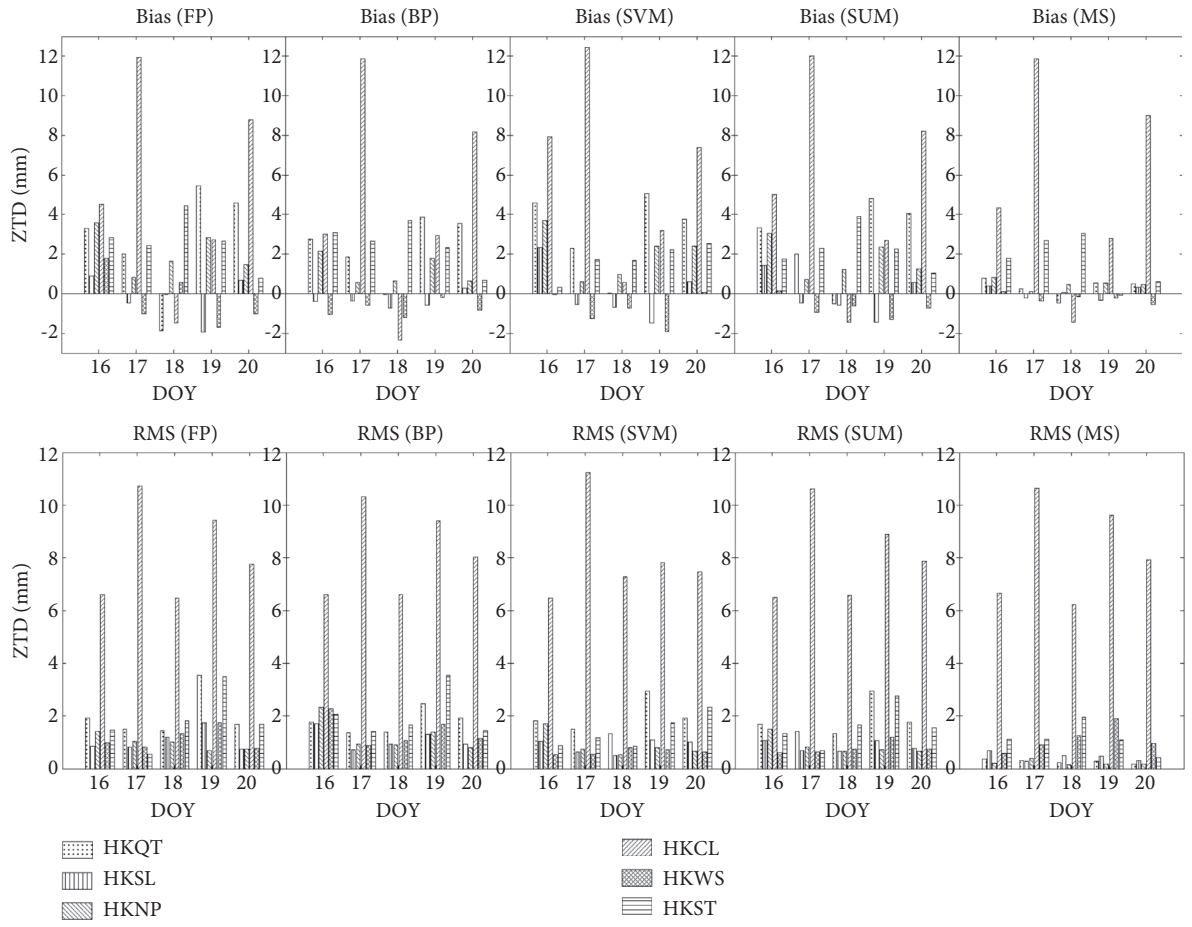

Figure 5: Daily fitting and forecast accuracy of the five models of real-time ZTD modeling, with real-time ZTD as the true value.

Table 4: Fitting and forecast accuracy statistical results of the five model for five consecutive days of real-time ZTD modeling, with real-time ZTD as the true value.

Modeling method	$\text{Bias}^{\text{observ}}$ (mm)			$\text{Bias}^{\text{true}}$ (mm)			STD (mm)			RMSE (mm)		
	HKQT	HKSL	HKNP	HKCL	HKWS	HKST	HKQT	HKSL	HKNP	HKCL	HKWS	HKST
FP	2.69	−0.17	2.08	5.30	−0.27	2.63	2.02	1.06	0.98	8.20	1.13	1.80
BP	2.40	−0.36	1.16	4.73	−0.77	2.48	1.78	1.12	1.27	8.19	1.40	2.03
SVM	3.15	0.04	2.01	6.30	−0.78	1.69	1.90	0.85	0.89	8.05	0.64	1.39
SUM	2.74	−0.10	1.72	5.30	−0.68	2.26	1.82	0.85	0.87	8.09	0.78	1.60
MS	0.32	0.05	0.48	5.31	−0.23	1.61	0.28	0.45	0.22	8.21	1.11	1.14
Mean	2.26	−0.11	1.49	5.39	−0.55	2.13	1.56	0.87	0.85	8.15	1.01	1.59

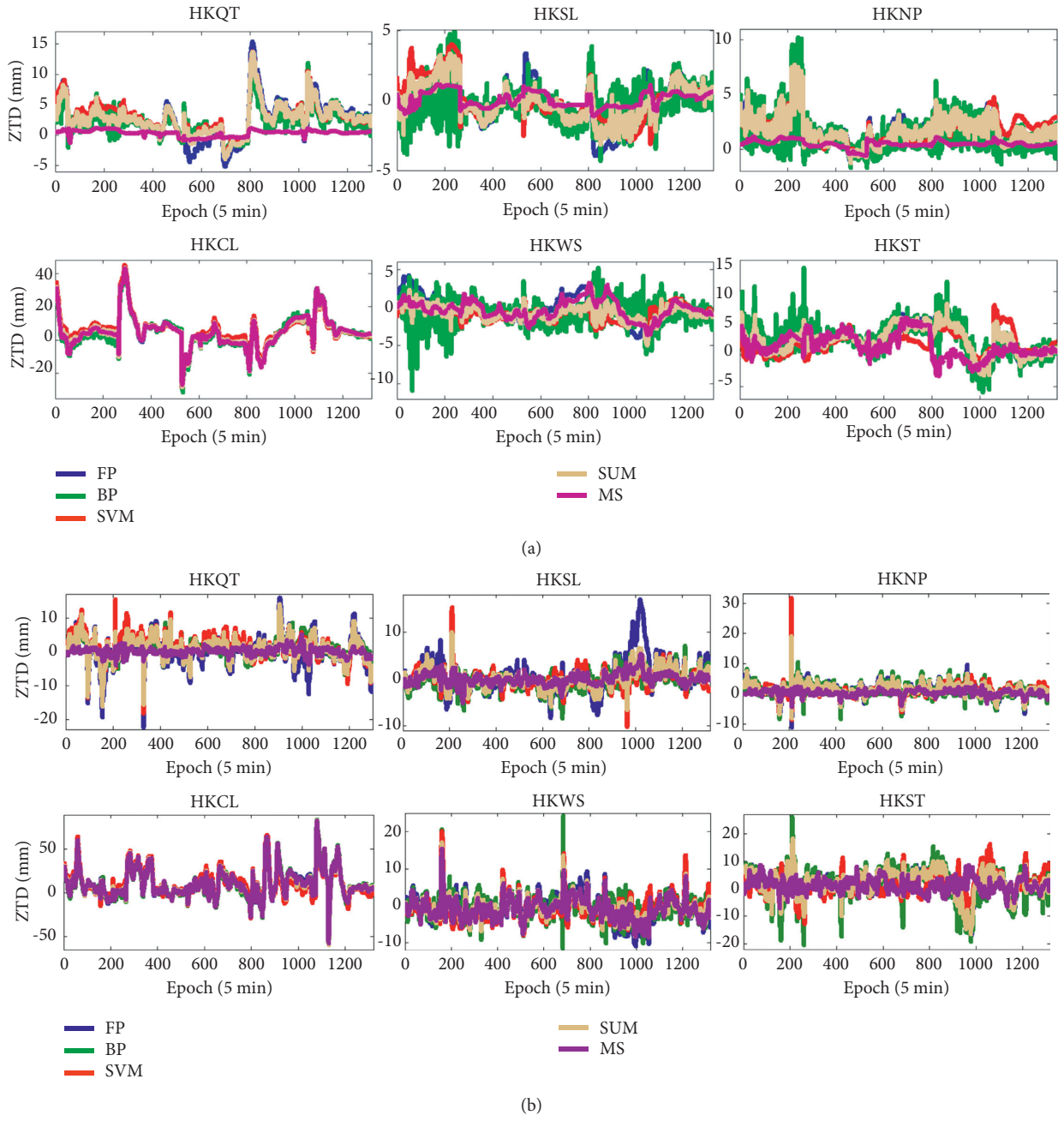

Figure 6: (a) Real-time and (b) final ZTD error changes of HKSL and HKWS stations for five consecutive days.

22.34%, respectively, compared with that of MS. RMS of FP, BP, SVM, and SUM for the real-time modeling of HKWS and HKST stations reduces by 38.55%, 41.16%, 36.55%, and 36.59%, respectively, compared with that of MS. For the bias accuracy of the four stations, the MS model also showed a similar improvement rate in the real-time and final modeling results compared with the four other models.

(b) Tables 2 and 4, Figures 6 and 7, and the analysis in (a) showed that the error distribution of real-time modeling is better than that of final modeling. RMS of real-time modeling for the FP, BP, SVM, SUM, and MS modeling of HKQT, HKSL, and HKNP stations improves by 57.03%, 32.29%, 52.39%, 48.52%, and 70.15%, respectively, compared with that of the final modeling. RMS of real-time modeling for the FP, BP, SVM, SUM, and MS modeling of HKCL, HKWS, and HKST stations improves by 55.21%, 51.86%, 64.52%, 59.19%, and 52.83%, respectively, compared with that of the final modeling. The modeling error analysis of the six stations for five consecutive days showed that the standard deviation and average value of real-time modeling improved by 43.19% and 24.04%, respectively, compared with those of the final modeling primarily because the stability of the station real-time ZTD before real-

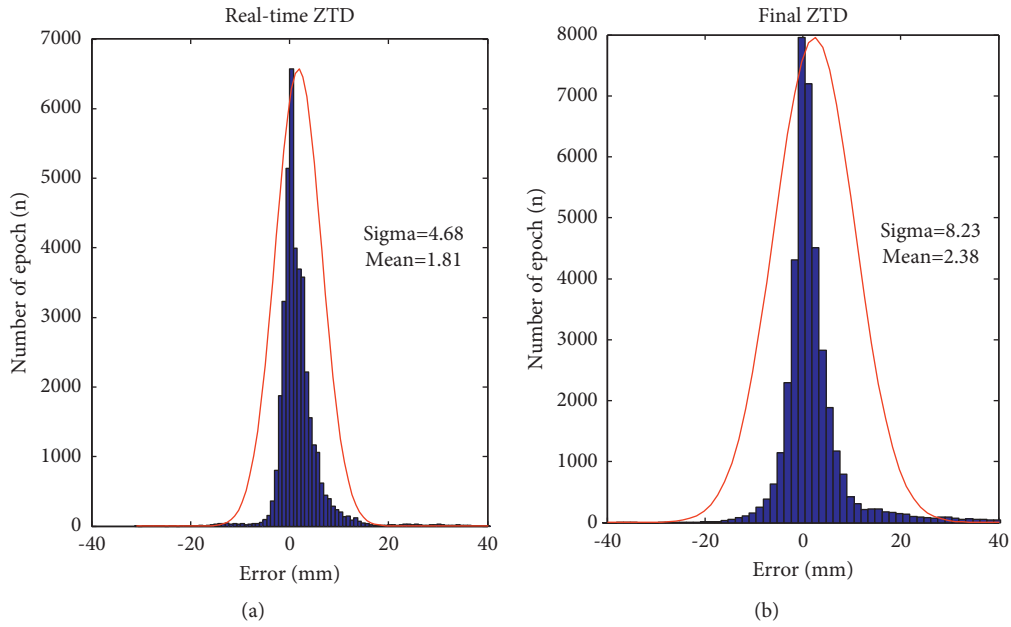

Figure 7: Error distribution of (a) real-time and (b) final ZTD modeling.

time ZTD modeling is better. ZTD is obtained using the real-time PPP solution with high-frequency real-time orbit and clock offset in a sampling interval of 5 s.

3.3. PPP Accuracy Verification. The HKQT, HKSL, HKNP, HKCL, HKWS, and HKST stations data in the 20th day of 2019 is selected, with 30 s sampling interval. The data of the first 2 h is not used. To validate the effectiveness of the MS modeling method, static PPP solution is carried out, with GPS and GLONASS satellite system observations, and precision orbit and clock offset products being the same as in Section 2.1. Four experimental schemes are designed: Scheme 1, PPP solution based on GBM final precision products; Scheme 2, based on Scheme 1, adding precise *a priori* constraint [19] (initial values of the final ZTD derived from MS modeling); Scheme 3, PPP solution based on CLK93 Real-time precision products; and Scheme 4, based on Scheme 3, adding precise *a priori* constraint (initial values of the real-time ZTD derived from MS modeling). Figure 8 shows the station HKST′ positioning results in N, E, and U components under the four schemes. Table 5 shows the positioning results, convergence time, and comparison under the four schemes for the six stations. The convergence criterion is defined as the moment when the error of positioning is less than 0.1 m in each component of N, E, and U.

The following can be deduced from Figure 8 and Table 5:

(a) In final PPP or real-time PPP, the positioning precisions or convergence time of the scheme with prior ZTD constraint is better than the scheme without the constraint. For the HKNP station, the positioning precisions of Scheme 2 is improved by 60.32%, 26.87%, and 3.00% in N, E, and U components, respectively, compared with the results of Scheme 1. The positioning precisions of Scheme 4 are improved by 72.06%, 8.71%, and 56.46% in N, E, and U components, respectively compared with the results of Scheme 3. For the HKST station, the convergence time of Scheme 2 is improved by 63.64%, 32.45%, and 19.15% in N, E, and U components, respectively, compared with the results of Scheme 1. The convergence time of Scheme 4 is improved by 53.23%, 25.49%, and 17.86% in N, E, and U components, respectively, compared with the results of Scheme 3. In general, the positioning precisions and convergence time of Scheme 2 are improved by 17.09%, 18.41%, 0.89%, 45.83%, 15.38%, and 33.88% in N, E, and U components, respectively, compared with the results of Scheme 1. The positioning precisions and convergence time of Scheme 4 are improved by 2.83%, 3.75%, 27.33%, 46.88%, 8.13%, and 18.22% in N, E, and U components, respectively, compared with the results of Scheme 3. The main reason for the improvement of PPP positioning performance is as follows. In general, ZTD changes slowly in the short term and can be obtained with high precision through the modeling method proposed in this paper. The addition of high-precision *a priori* ZTD increases the observation amount of PPP model and improves the accuracy and stability of the model.

(b) For the PPP solution with *a priori* ZTD constraint, the convergence time and positioning precisions of some stations are improved significantly in U component. For HKWS station, the convergence time and positioning precisions of Scheme 2 are improved by 80.00% and 7.76% in U component, respectively, compared with the results of Scheme 1. The convergence time and positioning precisions of Scheme 4 are improved by 57.89% and 56.46%, respectively,

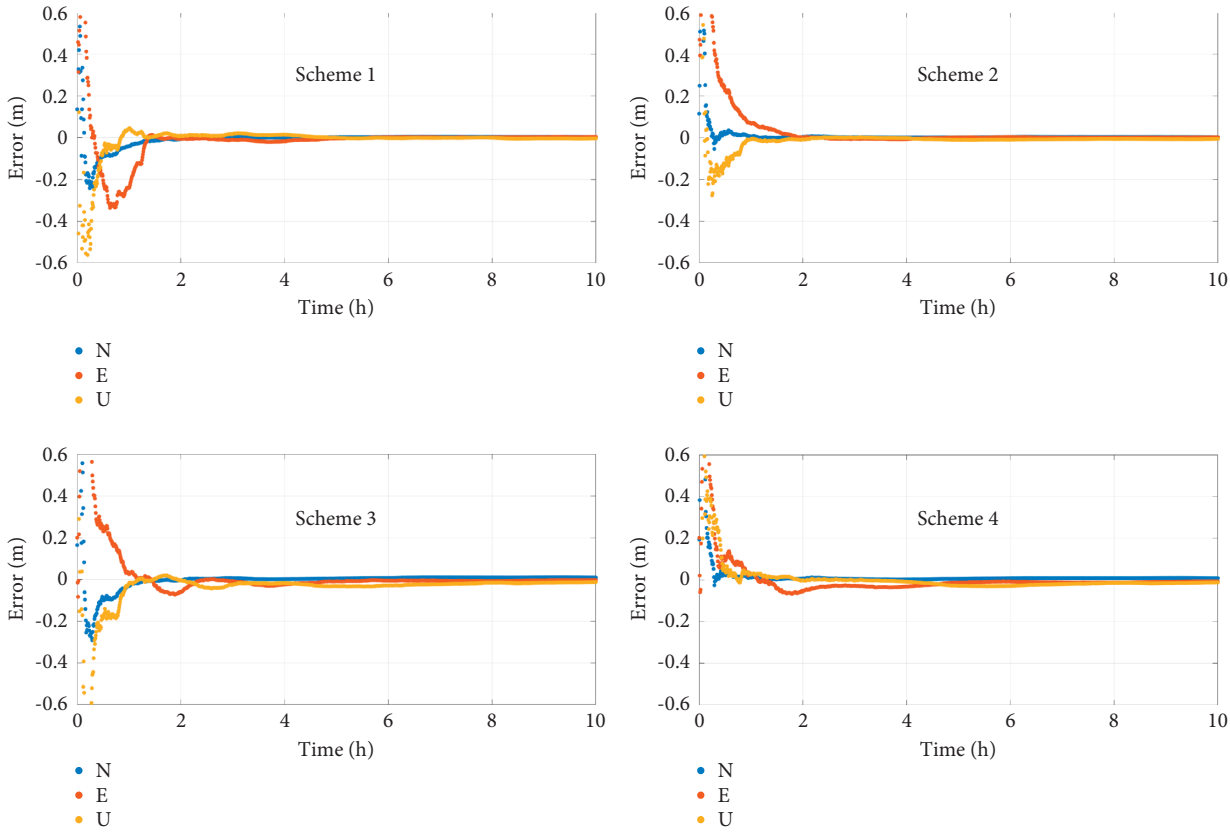

Figure 8: Static PPP positioning results of HKST station in four schemes at first 10 h.

Table 5: Statistical results of static and simulated dynamic PPP positioning results of all stations in four schemes and accuracy comparison between different schemes.

Station	Scheme 1 P (cm)/T (min)	Scheme 2 P (cm)/T (min)	Scheme 3 P (cm)/T (min)	Scheme 4 P (cm)/T (min)
HKQT	1.29/4.53/2.29/5.50/31.50/23.50	1.73/4.27/2.23/3.50/29.00/24.00	1.48/3.17/4.22/6.00/44.00/11.50	2.61/2.36/2.64/4.00/42.50/24.50
HKSL	1.66/7.64/1.69/8.50/13.00/14.00	1.95/5.94/1.67/4.50/12.50/4.00	1.78/2.87/2.92/10.00/32.00/6.50	3.00/3.05/2.18/4.50/27.50/8.50
HKNP	4.31/5.62/2.00/8.50/17.50/16.00	1.71/4.11/1.94/8.50/19.50/10.50	4.76/3.10/5.42/8.50/27.00/9.50	1.33/2.83/2.36/8.50/30.50/4.00
HKCL	5.99/5.33/9.74/5.50/23.00/24.00	6.11/4.98/9.41/8.50/23.00/18.50	6.15/8.60/9.10/6.00/35.50/29.50	6.18/8.55/9.02/6.50/32.50/14.50
HKWS	2.07/3.57/2.19/16.50/8.50/20.00	1.99/2.81/2.02/4.00/8.00/4.00	2.12/3.65/3.01/18.50/32.00/27.50	2.73/3.04/1.56/4.50/32.50/17.50
HKST	1.36/4.71/1.29/27.50/75.50/23.50	0.34/3.51/1.76/10.00/51.00/19.00	0.70/1.56/1.64/31.00/51.00/28.00	0.66/2.26/1.36/14.50/38.00/23.00
Average	2.78/5.23/3.20/12.00/28.17/20.17	2.31/4.27/3.17/6.50/23.83/13.33	2.83/3.83/4.39/13.33/36.92/18.75	2.75/3.68/3.19/7.08/33.92/15.33
Improvement rate	—/—/—/—/—/—	17.09/18.41/0.89/45.83/15.38/33.88	—/—/—/—/—/—	2.83/3.75/27.33/46.88/8.13/18.22

Note. P and T are the positioning precision and the convergence time in N, E, and U components, respectively. Improvement rate describes the improvement effect of the PPP solution with ZTD constraint compared with the solution without constraint, in unit of %.

compared with the results of Scheme 3. The main reason is that the position parameter in U component in the PPP model is correlated with ZTD parameter and the addition of high-precision *a priori* ZTD can accelerate the convergence time of ZTD parameter and improve the precision of ZTD. Then, the positioning performance in U component is improved.

(c) In all schemes, the positioning precision of static PPP can reach cm level. On the whole, the positioning performance of real-time PPP is not much different

from that of final PPP. The main reason is that there is little difference between the accuracy of high-frequency CLK93 real-time products and GBM final products used in this paper.

4. Summary and Discussion

Real-time and final ZTD values of 19 stations for five consecutive days in the Hong Kong CORS network are first obtained in this study by using the PPP solution. Five ZTD modeling methods (FP, BP, SVM, SUM, and MS models) are used to carry out regional real-time and final ZTD modeling. Finally, real-time and final ZTD fitting and prediction accuracy values are analyzed. The following conclusions can be drawn from this study:

(1) MS based on the genetic optimization algorithm demonstrates better learning and generalization abilities than other models.

(2) All five methods show high accuracy in the final ZTD modeling. Minimum, maximum, and average values of average bias for five consecutive days are 0.0022 (SVM), 2.21 (FP), and 0.67 mm, respectively. Minimum, maximum, and average values of average RMS are 0.97 (MS), 4.88 (BP), and 2.67 mm, respectively.

(3) All five methods exhibit high accuracy in real-time ZTD modeling. Minimum, maximum, and average values of average bias for five consecutive days are 0.04 (SVM), 3.15 (SVM), and 1.09 mm, respectively. Minimum, maximum, and average values of average RMS are 0.22 (MS), 2.03 (BP), and 1.18 mm, respectively.

(4) The SVM and SUM models present a significant advantage over the FP and BP models in modeling the station with elevation at the average level of the survey area.

(5) The error distribution of real-time modeling is significantly better than that of the final modeling, being taken the real-time and final PPP-based ZTD as the true values, respectively. STD and the average value of real-time modeling improved by 43.19% and 24.04% compared with those of the final modeling.

(6) Adding the ZTD derived from the multicore support vector machine regional ZTD modeling, the positioning precisions and convergence time of real-time PPP solution are improved by 2.83%, 3.75%, 27.33%, 46.88%, 8.13% and 18.22% in N, E, and U components, respectively.

The high accuracy real-time modeling of the regional tropospheric delay in this study can provide a theoretical reference for real-time PPP research based on regional atmospheric enhancement products. Meanwhile, the neural network model based on the genetic algorithm can be used to optimize the BP model in this study and reduce the occurrence of the network falling into the local optimal value. The time factor taken as the reference value can be the input to the neural network or SVM training center to improve the modeling accuracy further. An increasingly correct elevation naturalization model can be introduced to improve the modeling accuracy.

Data Availability

The data used to support the findings of this study are available from the corresponding author upon request.

Conflicts of Interest

The authors declare no conflicts of interest.

Authors' Contributions

Xu Yang and Xinyuan Jiang conceived and defined the research scheme. Xu Yang and Chuang Jiang verified the feasibility of the method and implemented the software algorithm. Xu Yang and Lei Xu checked the data processing results and wrote the manuscript. Chuang Jiang and Lei Xu helped to revise the manuscript and modified some figures and tables.

Acknowledgments

This work was supported by "Key Natural Science Projects of Anhui Provincial Department of Education (KJ2020A0311)," "Introduction of Talent Research Startup Fund Project of Anhui University of Science and Technology," "Open Fund Project of Coal Industry Engineering Research Center of Mining Area Environmental and Disaster Cooperative Monitoring in 2020 (KSXTJC202005)," and "Key Research and Development Projects of Anhui Province (202104a07020014)," and Hong Kong CORS network is acknowledged for providing data.

References

[1] Y. Yao, C. Xu, J. Shi, N. Cao, B. Zhang, and J. Yang, "ITG: a new global GNSS tropospheric correction model," *Scientific Reports*, vol. 5, no. 10273, pp. 1–9, 2015.

[2] J. Kouba and P. Héroux, "Precise point positioning using IGS orbit and clock products," *GPS Solutions*, vol. 5, no. 2, pp. 12–28, 2001.

[3] A. E. Niell, A. J. Coster, F. S. Solheim et al., "Comparison of measurements of atmospheric wet delay by radiosonde, water vapor radiometer, GPS, and VLBI," *Journal of Atmospheric and Oceanic Technology*, vol. 18, no. 6, pp. 830–850, 2001.

[4] L. Huang, G. Zhu, L. Liu, H. Chen, and W. Jiang, "A global grid model for the correction of the vertical zenith total delay based on a sliding window algorithm," *GPS Solutions*, vol. 25, no. 98, pp. 1–14, 2021.

[5] X. Li, X. Zhang, and M. Ge, "Regional reference network augmented precise point positioning for instantaneous ambiguity resolution," *Journal of Geodesy*, vol. 85, no. 3, pp. 151–158, 2011.

[6] H. Zhang, Y. Yuan, W. Li, B. Zhang, and J. Ou, "A grid-based tropospheric product for China using a GNSS network," *Journal of Geodesy*, vol. 92, no. 7, pp. 765–777, 2018.

[7] W. Dai, Z. Cheng, and C. Kuang, "Modeling regional precise tropospheric delay," *Geomatics and Information Science*, vol. 36, no. 4, pp. 392–396, 2011.

[8] H. Lv, W. Huang, and D. Wen, "A tropospheric delay prediction model based on spectrum analysis and the AR compensation," *Journal of Geodesy and Geodynamics*, vol. 35, no. 2, pp. 283–286, 2015.

[9] J. Ma, Y. Tao, and W. Yin, "Interpolation model of GPS tropospheric delay based on RBF neural network," *Metal Mine*, vol. 496, no. 10, pp. 33–35, 2017.

[10] D. Y. Zheng, W. S. Hu, J. Wang, and M. C. Zhu, "Research on regional zenith tropospheric delay based on neural network technology," *Survey Review*, vol. 47, no. 343, pp. 286–295, 2015.

[11] G. Xiao, J. Ou, G. Liu, and H. Zhang, "Construction of a regional precise tropospheric delay model based on improved BP neural network," *Chinese Journal of Geophysics*, vol. 61, no. 8, pp. 3139–3148, 2018.

[12] Y. Chen, W. Hu, Y. Yan, F. Long, and L. Zhang, "Research on tropospheric delay model based on neural network model error compensation technique," *Journal of Geodesy and Geodynamics*, vol. 38, no. 6, pp. 577–580, 2018.

[13] J. Deng, M. Xu, X. Yu, and A. Zhang, "Interpolation estimation method of tropospheric delay for long baseline network RTK based on support vector machine," *IOP Conference Series: Earth and Environmental Science*, vol. 192, pp. 1–9, Article ID 012069, 2018.

[14] S. Li, T. Xu, N. Jiang, H. Yang, and Z. Zhang, "Regional zenith tropospheric delay modeling based on least squares support vector machine using GNSS and ERA5 data," *Remote Sensing*, vol. 13, no. 1004, pp. 1–18, 2021.

[15] L. Lin, Z. Zhao, Q. Zhu, and Y. Zhang, "Profiling tropospheric refractivity in real time, based on a relevance vector machine and single ground-based GPS receiver," *International Journal of Remote Sensing*, vol. 33, no. 13, pp. 4044–4058, 2012.

[16] M. Sangiorgio, S. Barindelli, R. Biondi, E. Solazzo, and G. Guariso, "Improved extreme rainfall events forecasting using neural networks and water vapor measures," in *Proceedings of the 6th International Conference on Time Series and Forecasting (ITISE 2019)*, Granada, Spain, September 2019.

[17] R. Shamshiri, M. Motagh, H. Nahavandchi, M. H. Haghighi, and M. Hoseini, "Improving tropospheric corrections on large-scale sentinel-1 interferograms using a machine learning approach for integration with gnss-derived zenith total delay (ZTD)," *Remote Sensing of Environment*, vol. 239, no. 111608, pp. 1–4, 2020.

[18] Y. Yao, C. He, B. Zhang, and C. Xu, "A new global zenith tropospheric delay model GZTD," *Chinese Journal of Geophysics*, vol. 56, no. 7, pp. 2218–2227, 2013, in Chinese.

[19] Y. Yao, C. Yu, and Y. Hu, "A new method to accelerate PPP convergence time by using a global zenith troposphere delay estimate model," *Journal of Navigation*, vol. 67, no. 5, pp. 899–910, 2014.

[20] X. Li, *Rapid Ambiguity Resolution in GNSS Precise Point Positioning*, Wuhan University, Wuhan, China, 2013.

[21] Z. Dai, *GNSS Real-Time Precise Positioning Service System: Theory, Algorithm and Implementation*, Wuhan University, Wuhan, China, 2016.

[22] X. Yang, G. Chang, Q. Wang, S. Zhang, Y. Mao, and X. Chen, "An adaptive kalman filter based on variance component estimation for a real-time ZTD solution," *Acta Geodaetica et Geophysica*, vol. 54, no. 1, pp. 89–121, 2019.

[23] C. Cortes and V. Vapnik, "Support-vector networks," *Machine Learning*, vol. 20, no. 3, pp. 273–297, 1995.

[24] J.-T. Jeng, "Hybrid approach of selecting hyperparameters of support vector machine for regression," *IEEE Transactions on Systems, Man, and Cybernetics, Part B (Cybernetics)*, vol. 36, no. 3, pp. 699–709, 2006.

[25] Z. Chen, J. Li, L. Wei, W. Xu, and Y. Shi, "Multiple-kernel SVM based multiple-task oriented data mining system for gene expression data analysis," *Expert Systems with Applications*, vol. 38, no. 10, pp. 12151–12159, 2011.

[26] F. R. Bach, G. R. G. Lanckriet, and M. I. Jordan, "Multiple kernel learning, conic dualityand the SMO algorithm," in *Proceedings of the Twenty First International Conference on Machine Learning*, Banff, Canada, July 2004.

[27] Z.-P. Wu and X.-G. Zhang, "Elastic multiple kernel learning," *Acta Automatica Sinica*, vol. 37, no. 6, pp. 693–699, 2011.

[28] Y. Wan, H. Tong, and Y. Zhu, "Parameters optimization of multi-kernel support vector machine based on genetic algorithm," *Journal of Wuhan University of Technology (Natural Sciences Education)*, vol. 58, no. 3, pp. 255–259, 2012.

[29] C. Qian, C. He, and H. Liu, "Regional precise troposphere delay modeling based on spherical cap harmonic analysis," *Acta Geodaetica et Cartographica Sinica*, vol. 43, no. 3, pp. 248–256, 2014.

[30] Q. Chen, S. Song, S. Heise, Y.-A. Liou, W. Zhu, and J. Zhao, "Assessment of ZTD derived from ECMWF/NCEP data with GPS ZTD over China," *GPS Solutions*, vol. 15, no. 4, pp. 415–425, 2011.

[31] X. Li, M. Ge, H. Zhang, T. Nischan, and J. Wickert, "The GFZ real-time GNSS precise positioning service system and its adaption for COMPASS," *Advances in Space Research*, vol. 51, no. 6, pp. 1008–1018, 2013.

[32] X. Yang, Q. Wang, and W. Lyu, "A real-time clock offset prediction algorithm based on satellite clock offset autocorrelation," *Science of Surveying and Mapping*, vol. 46, no. 1, pp. 24–35, 2021.